Chemistry Europe
European Chemical Societies Publishing

WILEY VCH

Excellence in Chemistry Research

Announcing our new flagship journal

- Gold Open Access
- Publishing charges waived
- Preprints welcome
- Edited by active scientists

Meet the Editors of *ChemistryEurope*

Luisa De Cola
Università degli Studi di Milano Statale, Italy

Ive Hermans
University of Wisconsin-Madison, USA

Ken Tanaka
Tokyo Institute of Technology, Japan

EurJIC
European Journal of Inorganic Chemistry

Research Article
doi.org/10.1002/ejic.202300313

Chemistry Europe
European Chemical Societies Publishing

www.eurjic.org

Special Collection

Slow Inversion of Coordinated Thioether Groups in SNS-Type Ruthenium Pincer Complexes

Frederik Rummel,[a] Frerk Wehmeyer,[a] Matthias Vogt,[a] and Robert Langer*[a]

The thioether-group-containing SNS-type pincer complex [({$EtSCH_2CH_2$}$_2$NH)RuCl(H)(PPh_3)] (**2**) exists in three different diastereomers (**2 a**–**c**). The molecular structures obtained from single crystal X-Ray diffraction studies of all three isomers reveal a difference in the relative orientation of the respective EtS-groups, while other commonly observed diastereomers as the result of *cis*-/*trans*- or *fac*-/*mer*-isomerism are not observed. Chemical exchange between the three diastereomers **2 a**–**c** was discovered by phase-sensitive ^{1}H and ^{31}P NOESY NMR spectroscopy, and further quantified by line shape analysis of ^{1}H NMR spectra. The experimentally derived averaged Gibbs energies of activation for the interconversion of the isomers (65–70 kJ/mol) are in good agreement with the results obtained from DFT calculations, which suggest an inversion of the ligating sulfur atoms, although a dissociative pathway for the configurational inversion can be competitive.

Thioethers are common neutral ligands in transition metal complexes,[1] which are often used as easily replaceable monodentate ligands or Lewis bases in complexes like $AuCl \cdot SMe_2$ or reagents like $ClH_2B \cdot SMe_2$. In chelating ligands thioethers have raised increasing attention as stabilizing σ-donating groups for thiophilic transition metals in lower oxidation states[2–4] and as hemilabile groups in metal catalysts.[5,6] In particular the utilization of thioether groups in pincer-type ligands led to active catalysts[7] utilized for the hydrogenation of carbonyl compounds or dehydrogenation of alcohols,[8–17] ester metathesis,[8] alkane transfer-hydrogenation,[18] cross coupling,[19] cycloaddition[20] and ethylene oligomerization reactions[21–23] in recent years.

In particular, SN^{H}S-type pincer ligands, featuring a central amine group, are discussed as highly active, more air-stable and less electron-rich alternatives to commonly utilized PN^{H}P-type ligands in ruthenium catalysts for (de)hydrogenation catalysis. However, due to the center of chirality at the ligating sulfur atom, generated upon coordination of the thioether groups, the number of possible ligand arrangements and isomers is increased,[24,25] which potentially can lead to a stabilization of a less active or an inactive isomer. An inherent feature of non-symmetric thioether groups of the type R^1-S-R^2 is that a center of chirality is generated at the sulfur atom upon coordination to a transition metal (Figure 1 top). However, the barrier for the chiral inversion at the sulfur atom of coordinated thioether groups is in range of 40 to 60 kJ/mol and therefore often too low to yield configurationally stable complexes with this class of ligands.[2]

Based on our previous investigations on hydrogenation and dehydrogenation catalysts with pincer-type ligands,[26–31] we started to focus on SNS-type ligands in potentially improved catalysts for various reactions involving dihydrogen. In previous reports, the development of active catalysts for the hydrogenation of carbonyl compounds or the dehydrogenation of alcohols included SNS-type ruthenium pincer complexes, which are often obtained as a mixture of not fully characterized isomers.[8,32] Depending on the ancillary ligands neighboring the tridentate SNS-type ligand, a number of isomers can be theoretically formed in addition to stereo isomers with different configurations at the sulfur atoms (Figure 1 bottom) including for instance a *fac*- or *mer*-coordination of the SNS-ligand, different *cis*-/*trans*-arrangements of ancillary ligands in *e.g.* octahedral coordination modes, as well as different *cisoide* or *transoide* orientation modes of the central donor groups with formally sp^3-hybridized ligating atoms, such as amines, relative to an ancillary apical ligand. In view of the relatively high number of possible isomers and their impact on the performance in catalytic reactions, we started to investigate the identity

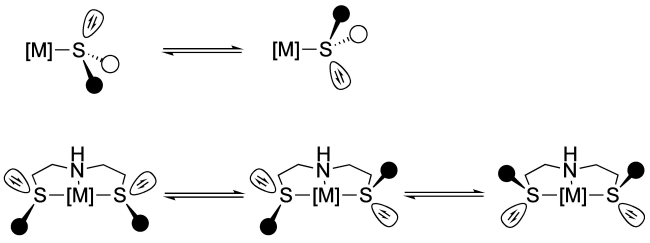

Figure 1. Configurational inversion at sulfur of non-symmetrical monodentate thioether ligands (top) in the coordination sphere of a metal center vs. the inversion in amine-based SNS-type pincer ligands (bottom).

[a] *F. Rummel, F. Wehmeyer, Dr. M. Vogt, Prof. Dr. R. Langer*
Institute of Chemistry
Faculty of Natural Sciences II
Martin-Luther-University Halle- Wittenberg
Kurt-Mothes-Str. 2
06120 Halle (Saale) (Germany)
E-mail: robert.langer@chemie.uni-halle.de

Supporting information for this article is available on the WWW under https://doi.org/10.1002/ejic.202300313

Special Collection *Part of the Special Collection on "Inorganic Reaction Mechanisms".*

Research Article
doi.org/10.1002/ejic.202300313

Chemistry Europe
European Chemical Societies Publishing

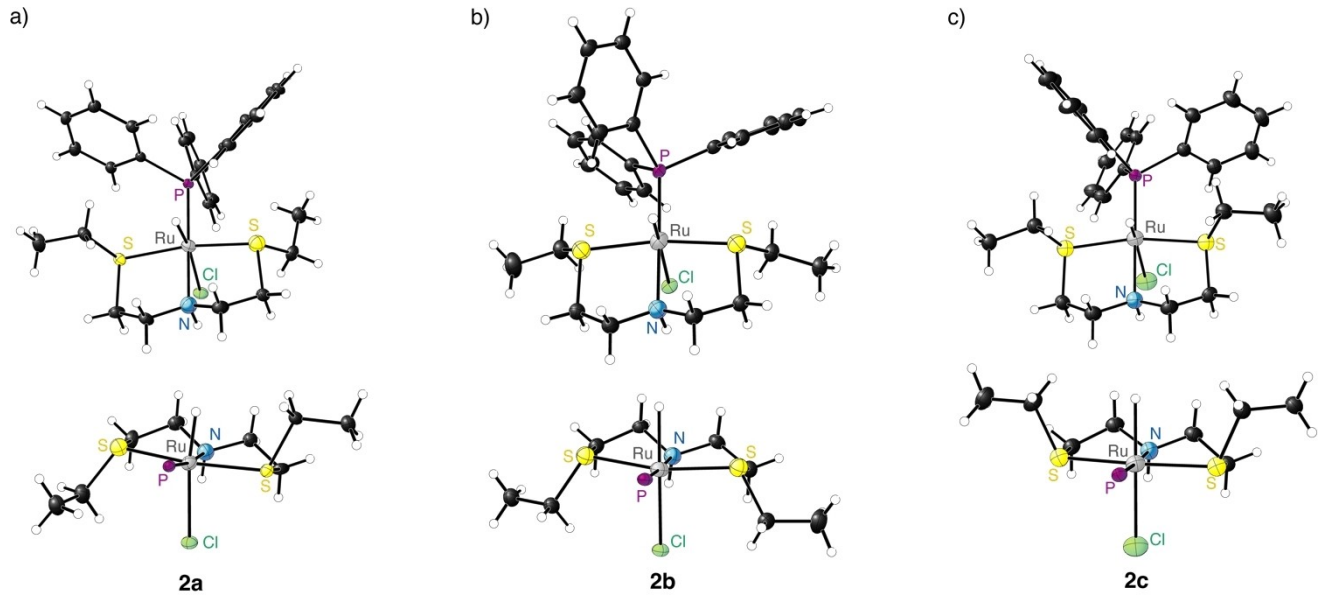

Figure 2. Different orientations of the molecular structures of the isomeric complexes **2a**, **2b** and **2c** in the solid state (derived from SC-XRD analysis, thermal ellipsoids are drawn at 50% probability level, non-coordinated solvent molecules were omitted for clarity, in the front view representation in the bottom section the phenyl-groups of the ancillary PPh_3 groups are omitted for clarity, but are shown in the upper part).

of the isomers in more detail in an octahedral ruthenium(II) complex decorated with an SNS-pincer-type ligand.

Results and Discussion

The hydrido complex [({$EtSCH_2CH_2$}$_2$NH)RuCl(H)(PPh_3)] (**2**) was obtained by complexation of [$(Ph_3P)_3$Ru(H)Cl] with the SNS-ligand $HN(CH_2CH_2SEt)_2$ (**1**, Scheme 1), as previously reported by Gusev and co-workers.[17]

In line with the previous spectroscopic reports, three isomers (**2a–c**) are detected by $^{31}P\{^1H\}$ NMR spectroscopy with singlet resonances at chemical shifts of 63.9, 66.3 and 67.9 ppm for the ancillary PPh_3 ligand. The chemical shifts corresponding to the the resonances of the hydrido ligands in **2a–c** at −20.45 (d, $^2J_{HP}$ = 27.4 Hz), −20.19 (d, $^2J_{HP}$ = 25.8 Hz) and −19.54 (d, $^2J_{HP}$ = 24.8 Hz) suggest a very similar arrangement of ligands in these isomers, but structural information has not been reported so far. Similar observations were made for the corresponding dichloride complex [({$EtSCH_2CH_2$}$_2$NH)$RuCl_2$(PPh_3)] which is also obtained as a mixture of three isomers.[32]

Complex **2** can be isolated by layering a mixture of all isomers (**2a–c**) with *n*-hexane, which gives rise to different types of single crystals that were subjected to single crystal X-Ray diffraction (SC-XRD) analysis. In line with the detection of three isomers in solution, it was possible to isolate single crystals of three different isomers and to determine their molecular structures (Figure 2, Table 1). All three isomers (**2a–c**) contain an octahedrally coordinated ruthenium center with apical hydrido and chlorido ligands in mutual *trans*-position. The triphenylphosphine ligand is located in equatorial position together with the *meridional* coordinated tridentate SNS-type chelate ligand. In all three isomers the hydrogen atom of the central secondary amine group was located on the same side as the chlorido ligand (mutual *cisoide* arrangement). The Ru–Cl-distance in **2a–c** is ranging from 2.583 Å to 2.619 Å, whereas the Ru–P-distance was found between 2.253 Å and 2.258 Å. The *meridionally* coordinated SNS-ligand gives rise to very similar Ru–S- (2.313…2.337 Å) and Ru–N-distances (2.159…2.163 Å). Overall, the structural analysis reveals that the formation of the three isomers of the pincer-type complex **2** originates from the center of chirality at the sulfur atoms of the coordinated thioether groups. In case of complex **2a** a pair of enantiomers was detected in the crystal lattice, which is determined by the configuration at the two sulfur atoms and therewith by the relative orientation of the thioether ethyl groups. In complex **2a** the sulfur-bound ethyl groups face toward opposite directions and adopt an *anti*-arrangement with respect to the

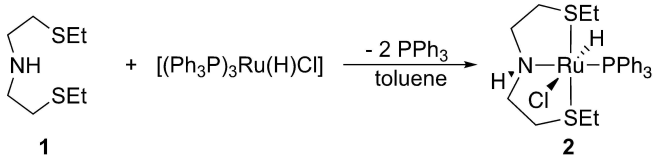

Scheme 1. Synthesis of complex **2**.

Table 1. Selected bond distances in the solid state of complexes **2a–c**.

Isomer	d_{Ru-Cl}/Å	d_{Ru-P}/Å	d_{Ru-N}/Å	d_{Ru-H}/Å	d_{Ru-S}/Å
2a	2.583(2)	2.254(2)	2.159(6)	1.64(6)	2.313(2) 2.335(2)
2b	2.583(1)	2.258(1)	2.163(2)	1.64(3)	2.321(1) 2.337(1)
2c	2.619(2)	2.253(1)	2.161(4)	1.607	2.334(1) 2.335(1)

Research Article
doi.org/10.1002/ejic.202300313

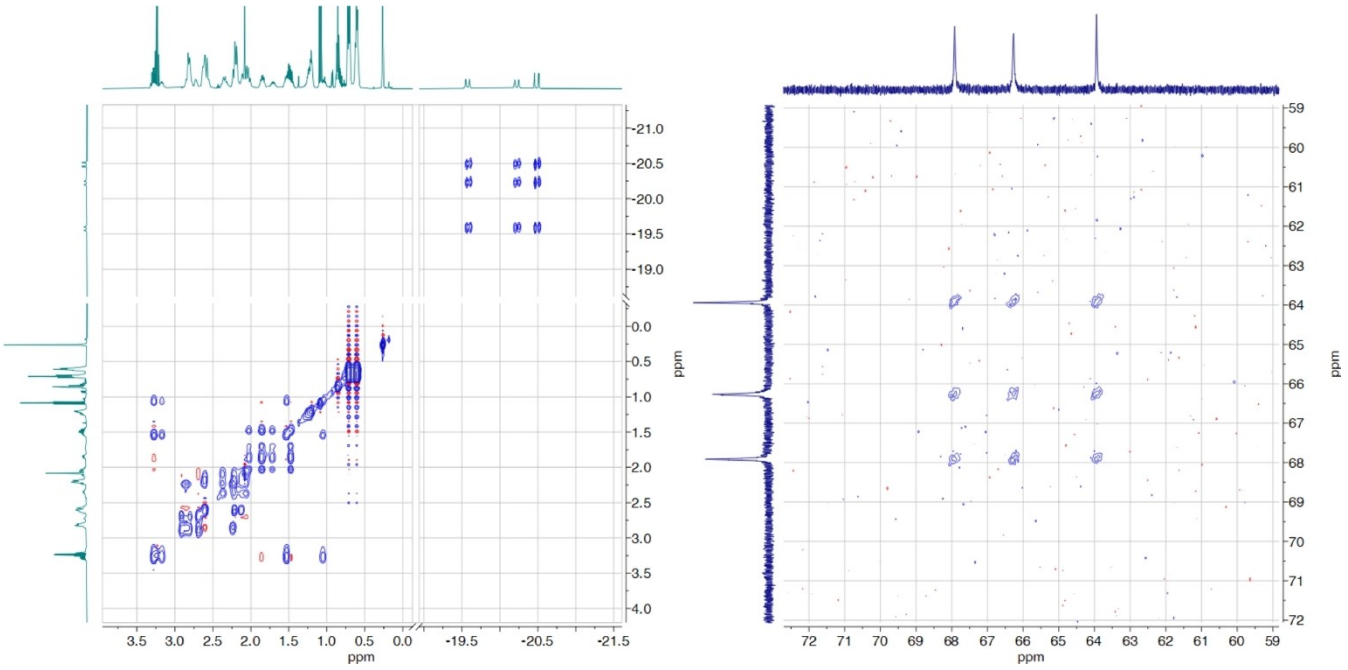

Figure 3. 2D $^{1}H^{1}H$ NOESY NMR spectrum (left) and 2D $^{31}P^{31}P$ NOESY NMR spectrum (right) of the isomers **2a–c** of complex **2** in C_6D_6 at 300 K.

central equatorial plane of the pincer ligand. (Fig 2, front view in the bottom section). In the two other detected isomers **2b** and **2c**, the two thioether ethyl groups are in a mutual *syn* arrangement, that is either both facing towards the ruthenium bound hydrido ligand (**2b**) or they are located on the same side as the chlorido ligand (**2c**), respectively.

The isolation and structural characterization of different isomers appears somewhat surprising and has not yet been reported, presumably because prochiral non-symmetric thioethers are known to undergo rapid racemization upon coordination to a metal center with barriers between 40 and 60 kJ/mol.[2]

As no significant broadening was observed in ^{1}H and $^{31}P\{^{1}H\}$ NMR spectra, a phase-sensitive ^{1}H NOESY NMR spectrum of complex **2** (Figure 3, left) was acquired, which displays significant cross-peaks for exchange correlations between the ^{1}H NMR resonances of all three isomers **2a–c**. In particular the diagnostic resonances corresponding to the hydrido ligands in **2a–c** indicate that the three isomeric species are in equilibrium. The findings are supported by ^{31}P NOESY NMR spectroscopy as well, as the spectrum exhibits cross-peaks indicative for exchange correlations between all isomers of **2** (Figure 3, right). The detection of three isomers of **2** in solution by NMR spectroscopy suggests that the observed resonances correspond to the three structurally characterized diastereomers in the solid state. However, it was not possible to make unambiguous assignments based on NOE cross peaks in the ^{1}H NOESY NMR spectrum, due to superimposed resonances of the diagnostic thioether ethyl groups.

Using line shape analysis of the resonances corresponding to the hydrido ligands of **2a–c** in ^{1}H NMR spectra (and for comparison in $^{1}H\{^{31}P\}$ NMR spectra), we extracted averaged rate constants for the exchange reaction (presumably via inversion of the configuration at the ligating sulfur atoms) at different temperatures in the range of 300 and 325 K. With well separated hydride resonances ($\delta_H = -19.57$, -20.22, -20.48 ppm) and limited line broadening ($W_{1/2} = 3$–22 Hz) in the 500 MHz ^{1}H NMR spectrum of **2a–c**, a slow exchange regime is assumed.[33,34]

As the ratio of equally sized integrals for the resonances of **2a**, **2b** and **2c** remains constant over the investigated temperature range a simple interpretation of the line broadening may be justified, although the underlying nature of k_{ex} might be quite complex, with scenarios for symmetric and non-symmetric three-state exchange. The Eyring analysis of k_{ex} ($k_{ex} = \pi \cdot \Delta\nu$) in the temperature range between 300 and 325 K reveals a linear dependence of ln(k/T) vs. 1/T and gives rise to similar activation parameters for the hydride resonances of **2a–c** (Table 2). Although the three hydride resonances exhibit different half height width values in the ^{1}H NMR spectrum, we used a simplified model for a symmetric three state exchange and assumed that all rate constants are equal ($k_{ex} = 4 \cdot k_{ab}$), which results in excellent correlations in the Eyring plot (Figure 4 right) and allows for a straight forward analysis of the line shape. The resulting averaged enthalpy of activation ranges

Table 2. Activation parameters for the exchange of **2a–c** derived from line shape analysis of NMR spectra.

δ_H/ppm	$\Delta H^{\neq}$/kJ·mol^{-1}	$\Delta S^{\neq}$/J·mol^{-1}·K^{-1}	$\Delta G^{\neq}$*(300 K)*/kJ·mol^{-1}
−19.57	59.2	−37.8	70.5
−20.22	61.9	−27.8	70.2
−20.48	56.0	−57.2	73.1

Research Article
doi.org/10.1002/ejic.202300313

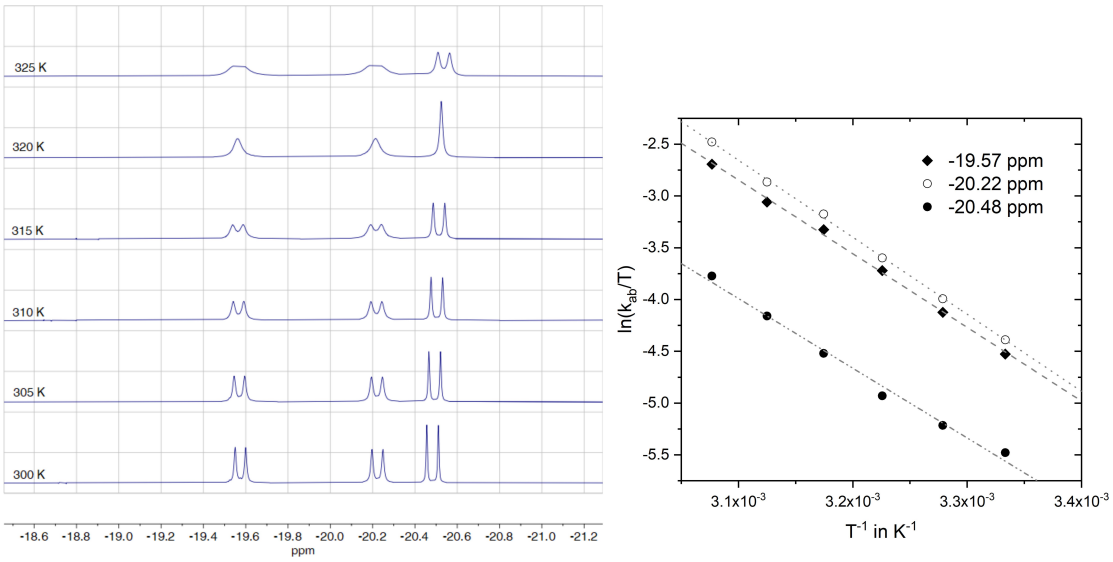

Figure 4. VT ^{1}H NMR spectra of **2a–c** in C_6D_6 at different temperatures (left) and the corresponding Eyring plot (right), which is based on line shape analysis.

from 56.0 to 61.9 kJ/mol, whereas the Gibbs energy of activation at 300 K was calculated to be between 70.2 and 73.1 kJ/mol. In comparison to coordinated monodentate thioether ligands (40 and 60 kJ/mol),[2] the values detected for the coordinated SNS-type pincer ligand in **2** are significantly higher, which might be one of the reasons for isolation and crystallographic characterization of the different isomers **2a–c**.

Quantum chemical investigations using density functional theory (DFT) were performed to gain further insights about the detected exchange reaction. For benchmarking geometry optimizations and subsequent frequency calculations were performed for **2a–c** with different functionals (B97D3,[35,36] M06L,[37] BP86,[38,39] B3LYP,[40–42] B3LYP-D3,[35] TPSSTPSS[43] and ωb97x-D[44]) and the def2-TZVP basis set.[45,46] It becomes evident that with functionals like B97D3 the Ru–Cl bond distance in the optimized geometries was significantly longer (2.9 vs. 2.6 Å) than in the experimentally derived molecular structure. With all functionals isomer **2b** was slightly more stable in Gibbs energy by −4.9 to −8.8 kJ/mol with respect to **2a**, whereas for **2c** it depends on the functional with differences in Gibbs energy ranging from −6.6 kJ/mol to 2.1 kJ/mol with respect to **2a** (Table 3). Considering the accuracy of DFT methods, the calculated values are in good agreement with the experimental results, which indicated a small or no difference in Gibbs energy for the three isomers.

Other isomers of **2a–c** with a *meridional* arrangement of the SNS-type ligand were calculated to be 48.3 to 68.9 kJ/mol higher in Gibbs energy with respect to **2a**, whereas isomers with a *facial* coordination mode of the SNS-type ligands are calculated to be 29.9 to 56.3 kJ/mol higher in Gibbs energy with respect to **2a** (with the B3LYP functional).

Transition states connecting **2a** with **2b** ($\mathbf{TS_{2a/2b}}$) and **2a** with **2c** ($\mathbf{TS_{2a/2c}}$) were located, which are characterized by a trigonal planar environment of one sulfur atom (Figure 5), as expected for an inversion of the center of chirality at the sulfur atom. However, it was not possible to locate a transition state for the direct conversion of **2b** into **2c** and back, which would involve the concerted inversion at both coordinated sulfur atoms. Inspection of the calculated Gibbs energies of activation and enthalpies of activation reveals that $\mathbf{TS_{2a/2b}}$ is at least 20 kJ/mol higher in Gibbs energy than $\mathbf{TS_{2a/2c}}$ for all functionals, with

Table 3. Relative values for ΔH/ΔG in kJ/mol obtained by DFT calculations with def2-TZVP basis set and different functionals.

Functional	$\mathbf{TS_{2a/2b}}$	**2b**	$\mathbf{TS_{2a/2c}}$	**2c**
B97D3	109.6/105.2	−3.5/−7.0	83.5/78.9	8.1/1.5
M06L	94.4/92.7	−0.6/−6.5	72.9/67.7	6.8/2.1
BP86	90.0/86.1	−7.3/−8.6	69.6/65.8	−1.4/−6.1
B3LYP	87.6/83.8	−8.0/−8.8	65.7/60.6	−2.9/−6.6
B3LYP-D3	102.1/98.5	−3.2/−6.1	73.5/67.2	4.0/−1.8
TPSSTPSS	89.0/86.9	−6.6/−7.8	62.4/58.2	−1.4/−6.0
wb97xd	100.2/95.6	−2.6/−4.9	74.3/72.0	3.4/−2.4

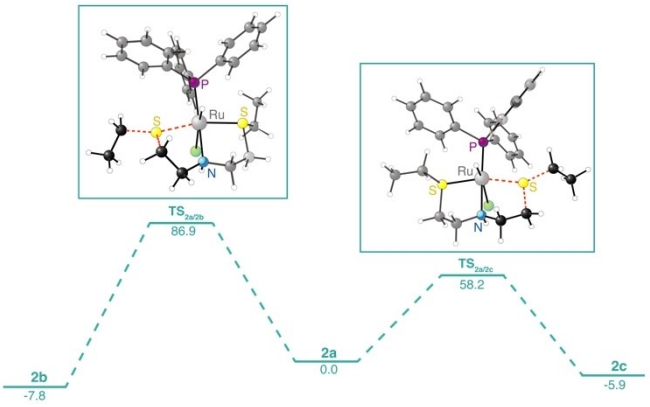

Figure 5. Calculated pathway for the interconversion of the stereoisomers **2a**, **2b** and **2c** based on density functional theory (DFT, exemplary shown for TPSSTPSS/ def2-TZVP) in kJ/mol.

Research Article
doi.org/10.1002/ejic.202300313

the values ranging for $\mathbf{TS_{2a/2b}}$ from 87.6 kJ/mol (B3LYP) to 109.6 kJ/mol (B97D3) and for $\mathbf{TS_{2a/2c}}$ from 62.4 kJ/mol (TPSSTPSS) to 83.5 kJ/mol (B97D3).

We tried to evaluate the performance of the different functionals by comparison of the averaged Gibbs energies of the two transition states $\mathbf{TS_{2a/2b}}$ and $\mathbf{TS_{2a/2c}}$ with the experimental results from the line shape analysis. In this context the TPSSTPSS- ($\overline{\Delta G^{\ddagger}} = 75.7$ kJ/mol) and the B3LYP-functional ($\overline{\Delta G^{\ddagger}} = 72.2$ kJ/mol) show the best agreement with the experimental results, whereas the B97D3- ($\overline{\Delta G^{\ddagger}} = 92.1$ kJ/mol) and wb97xd ($\overline{\Delta G^{\ddagger}} = 83.4$ kJ/mol) give rise to significantly higher values. These findings support that the observed chemical exchange in solution involves the three crystallographically characterized isomers **2a**–**c**.

Dissociation of one thioether group, as an alternative pathway for the formal inversion of the configuration at the ligating sulfur atom, was calculated to be thermodynamically uphill by 42.1 kJ/mol (**2a**), 49.0 kJ/mol (**2c**) and 61.3 kJ/mol (**2b**). For the most stable intermediate **2a'** after dissociation of one thioether group from **2a** a transition state was located with a Gibbs energy of 72.6 kJ/mol ($\mathbf{TS_{2a/2a'}}$). The rotation of the uncoordinated thioether group is necessary for a formal inversion at the sulfur atom after re-coordination, which proceeds via an additional transition state with a Gibbs energy of 68.4 kJ/mol ($\mathbf{TS_{2a'\text{-}rot}}$) with respect to **2a** (26.3 kJ/mol with respect to **2a'**).

Overall, the reported results indicate that the barriers for inversion at the sulfur atoms of coordinated non-symmetric thioether groups can be higher in pincer-type ligands, which allows for the isolation of different diastereomers in case of the investigated SNS-type pincer-ligands.

Conclusions

In conclusion we described a rare example of structurally characterized isomeric thioether complexes, differing solely in their configuration at the sulfur atoms. The line shape analysis in combination with quantum chemical investigations suggest that the three isolated isomers **2a**–**c** interconvert in solution, but with rather high barriers for the inversion of the coordinated thioether groups. As pincer-type ligands with thioether groups can lead to a significant improvement of catalyst activity in reactions like (de)hydrogenations, the reported results are of relevance for catalyst design and we currently investigate the impact of such inversion reactions in potential side equilibria on the overall catalytic performance.

Experimental Section

General Procedures: All experiments were carried out under purified argon atmosphere using standard Schlenk techniques. The solvents used were dried by standard methods and stored over appropriate molecular sieves under argon atmosphere.[47] NMR Spectra were recorded using an Agilent Technologies 500 MHz DD2 spectrometer at 300, 305, 310, 315, 320 and 325 K. ^{1}H chemical shifts are reported in ppm referenced to tetramethylsilane. The residual proton resonance of the deuterated solvent was used as internal standard for ^{1}H NMR spectra. ^{31}P NMR chemical shifts are reported in ppm downfield from H_3PO_4 and referenced to an external 85% solution of phosphoric acid in D_2O. The following abbreviations are used for the description of NMR data: br (broad), s (singlet), d (doublet), t (triplet), m (multiplet).

$[RuHCl(PPh_3)_3]$ and $(EtSC_2H_4)_2NH$ (**1**) were prepared according to known methods.[17,48] $[RuHCl(PPh_3)\{(EtSC_2H_4)_2NH\}]$ (**2**) was prepared according to a modified literature synthesis[17] described below.

Synthesis of $[RuHCl(PPh_3)\{(EtSC_2H_4)_2NH\}]$ (2): $RuHCl(PPh_3)_3$ (97 mg; 0.105 mmol) and $(EtSC_2H_4)_2NH$ (**1**, 20 mg; 0.105 mmol) were dissolved in 3 mL toluene and the solution was heated at 100 °C for 2 h. After cooling, diethyl ether (2 mL) and *n*-hexane (2 mL) were added and the solution was left in a freezer. The crystallized product was filtered-off, washed with diethyl ether (5 mL) and dried under vacuum overnight to give the yellow product. Yield: 20 mg (32%). Single crystals of **2a**–**c** suitable for single crystal XRD were obtained by layering a C_6D_6 solution with *n*-hexane. Due to the different orientation of the SEt groups, the product was isolated as a mixture of three isomers (**2a**–**c**). ^{1}H NMR (500 MHz, C_6D_6, 300 K): $\delta = -20.45$ (d, $^2J_{HP} = 27.4$ Hz, Ru*H*), -20.19 (d, $^2J_{HP} = 25.8$ Hz, Ru*H*), -19.54 (d, $^2J_{HP} = 24.8$ Hz, Ru*H*), 0.64 (br t, $^3J_{HH} = 7.4$ Hz, CH_3), 0.74 (t, $^3J_{HH} = 7.5$ Hz, CH_3), 1.43–1.63 (m, CH_2), 1.66–1.94 (m, CH_2), 2.02–2.18 (m superimposed, CH_2), 2.18–2.30 (m, CH_2), 2.30–2.48 (m, CH_2), 2.53–2.93 (m, CH_2), 3.15–3.36 (m superimposed, CH_2), 5.00 (br, N*H*), 6.99–7.10 (m, phenyl-*H*), 7.10–7.22 (m superimposed, phenyl-*H*), 8.02 (t, $J = 8.6$ Hz, phenyl-*H*) 8.08–8.19 (m, phenyl-*H*) ppm. ^{31}P{^{1}H} NMR (202 MHz, C_6D_6, 300 K): $\delta = 62.0$ (s), 64.9 (s), 66.6 (s) ppm.

Computational Details: All reported structures were optimized by density functional theory (DFT)[49] with different functionals and the def2-TZVP basis set[45,46] in the gas phase using Gaussian16.[50] Frequency analysis calculations of optimized structures were performed at the same level of theory (def2-TZVP) to characterize the structures to be minima (no imaginary frequency) or transition states (one imaginary frequency). Intrinsic reaction coordinate calculations were performed to confirm that the located transition states are connecting the minimum structures. xyz-coordinates of all minima and transition states are available in the supporting information and as separate xyz-files.

Deposition Number(s) 2265296 (for **2a**), 2265295 (for **2b**), 2265294 (for **2c**) contain(s) the supplementary crystallographic data for this paper. These data are provided free of charge by the joint Cambridge Crystallographic Data Centre and Fachinformationszentrum Karlsruhe Access Structures service.

Supporting Information

The authors have cited additional references within the Supporting Information.[51–54]

Acknowledgements

R. L. is grateful to the Deutsche Forschungsgemeinschaft (DFG) for supporting this research (LA 2830/6-2) and for funding within the Heisenberg program (LA 2830/9-1). Open Access funding enabled and organized by Projekt DEAL.

Conflict of Interests

The authors declare no conflict of interest.

Data Availability Statement

The data that support the findings of this study are available in the supplementary material of this article.

Keywords: isomerization · pincer ligand · reaction mechanisms · ruthenium · thioether

[1] S. G. Murray, F. R. Hartley, *Chem. Rev.* **1981**, *81*, 365–414.
[2] A. M. Masdeu-Bultó, M. Diéguez, E. Martin, M. Gómez, *Coord. Chem. Rev.* **2003**, *242*, 159–201.
[3] J. Margalef, O. Pàmies, M. A. Pericàs, M. Diéguez, *Chem. Commun.* **2020**, *56*, 10795–10808.
[4] A. Das, M. Saha, S. Mandal, S. Das, K. Das Saha, T. K. Mondal, *New J. Chem.* **2023**, *47*, 4931–4943.
[5] J. Vila, M. Solà, T. Achard, S. Bellemin-Laponnaz, A. Pla-Quintana, A. Roglans, *ACS Catal.* **2023**, 3201–3210.
[6] A. L. Gushchin, N. Y. Shmelev, S. F. Malysheva, A. V. Artem'ev, N. A. Belogorlova, P. A. Abramov, N. B. Kompan'kov, E. Manoury, R. Poli, D. G. Sheven, R. Llusar, M. N. Sokolov, *New J. Chem.* **2018**, *42*, 17708–17717.
[7] M. R. Elsby, R. T. Baker, *Acc. Chem. Res.* **2023**, *56*, 798–809.
[8] A. Dubey, E. Khaskin, *ACS Catal.* **2016**, *6*, 3998–4002.
[9] Y. Shaalan, L. Boulton, C. Jamieson, *Org. Process Res. Dev.* **2020**, *24*, 2745–2751.
[10] J. Schörgenhumer, A. Zimmermann, M. Waser, *Org. Process Res. Dev.* **2018**, *22*, 862–870.
[11] X. Chen, Y. Jing, X. Yang, *Chem. A Eur. J.* **2016**, *22*, 1950–1957.
[12] M. J. Page, J. Wagler, B. A. Messerle, *Organometallics* **2010**, *29*, 3790–3798.
[13] D. G. Gusev, *ACS Catal.* **2016**, *6*, 6967–6981.
[14] P. Puylaert, R. van Heck, Y. Fan, A. Spannenberg, W. Baumann, M. Beller, J. Medlock, W. Bonrath, L. Lefort, S. Hinze, J. G. de Vries, *Chem. Eur. J.* **2017**, *23*, 8473–8481.
[15] B. M. Stadler, P. Puylaert, J. Diekamp, R. van Heck, Y. Fan, A. Spannenberg, S. Hinze, J. G. de Vries, *Adv. Synth. Catal.* **2018**, *360*, 1151–1158.
[16] P. A. Dub, R. J. Batrice, J. C. Gordon, B. L. Scott, Y. Minko, J. G. Schmidt, R. F. Williams, *Org. Process Res. Dev.* **2020**, *24*, 415–442.
[17] D. Spasyuk, S. Smith, D. G. Gusev, *Angew. Chem. Int. Ed.* **2013**, *52*, 2538–2542.
[18] X. Zhou, S. Malakar, T. Zhou, S. Murugesan, C. Huang, T. J. Emge, K. Krogh-Jespersen, A. S. Goldman, *ACS Catal.* **2019**, *9*, 4072–4083.
[19] A. Fiebor, R. Tia, B. C. E. Makhubela, H. H. Kinfe, *Beilstein J. Org. Chem.* **2018**, *14*, 1859–1870.
[20] J. Vila, M. Solà, T. Achard, S. Bellemin-Laponnaz, A. Pla-Quintana, A. Roglans, *ACS Catal.* **2023**, *13*, 3201–3210.
[21] K. Albahily, S. Gambarotta, R. Duchateau, *Organometallics* **2011**, *30*, 4655–4664.
[22] A. Jabri, C. Temple, P. Crewdson, S. Gambarotta, I. Korobkov, R. Duchateau, *J. Am. Chem. Soc.* **2006**, *128*, 9238–9247.
[23] D. S. McGuinness, P. Wasserscheid, W. Keim, D. Morgan, J. T. Dixon, A. Bollmann, H. Maumela, F. Hess, U. Englert, *J. Am. Chem. Soc.* **2003**, *125*, 5272–5273.
[24] S. Werkmeister, J. Neumann, K. Junge, M. Beller, *Chem. Eur. J.* **2015**, *21*, 12226–12250.
[25] D. N. Chirdon, S. P. Kelley, N. Hazari, W. H. Bernskoetter, *Organometallics* **2021**, *40*, 4066–4076.
[26] Y. Li, L. Maser, L. Alig, Z. Ke, R. Langer, *Dalton Trans.* **2021**, *50*, 954–959.
[27] A. Bäcker, Y. Li, M. Fritz, M. Grätz, Z. Ke, R. Langer, *ACS Catal.* **2019**, *9*, 7300–7309.
[28] L. Vondung, L. E. Sattler, R. Langer, *Chem. Eur. J.* **2018**, *24*, 1358–1364.
[29] L. Vondung, N. Frank, M. Fritz, L. Alig, R. Langer, *Angew. Chem. Int. Ed.* **2016**, *55*, 14450–14454.
[30] F. Schneck, M. Assmann, M. Balmer, K. Harms, R. Langer, *Organometallics* **2016**, *35*, 1931–1943.
[31] W. Xu, R. Langer, *Dalton Trans.* **2015**, *44*, 16785–16790.
[32] D. Spasyuk, S. Smith, D. G. Gusev, *Angew. Chem. Int. Ed.* **2013**, *52*, 2538–2542.
[33] P. S. Pregosin, *NMR in Organometallic Chemistry*, Wiley-VCH, Weinheim, **2012**, p. 279.
[34] I. R. Kleckner, M. P. Foster, *Biochim. Biophys. Acta Proteins Proteomics* **2011**, *1814*, 942–968.
[35] S. Grimme, S. Ehrlich, L. Goerigk, *J. Comput. Chem.* **2011**, *32*, 1456–1465.
[36] S. Grimme, *J. Comput. Chem.* **2006**, *27*, 1787–1799.
[37] Y. Zhao, D. G. Truhlar, *J. Chem. Phys.* **2006**, *125*, 194101–1–194101-18.
[38] A. D. Becke, *Phys. Rev. A* **1988**, *38*, 3098–3100.
[39] J. P. Perdew, *Phys. Rev. B* **1986**, *33*, 8822–8824.
[40] A. D. Becke, *J. Chem. Phys.* **1993**, *98*, 5648–5652.
[41] S. H. Vosko, L. Wilk, M. Nusair, *Can. J. Phys.* **1980**, *58*, 1200–1211.
[42] C. Lee, W. Yang, R. G. Parr, *Phys. Rev. B* **1988**, *37*, 785–789.
[43] J. Tao, J. P. Perdew, V. N. Staroverov, G. E. Scuseria, *Phys. Rev. Lett.* **2003**, *91*, 3–6.
[44] J. Da Chai, M. Head-Gordon, *Phys. Chem. Chem. Phys.* **2008**, *10*, 6615–6620.
[45] F. Weigend, R. Ahlrichs, *Phys. Chem. Chem. Phys.* **2005**, *7*, 3297–3305.
[46] F. Weigend, C. Hättig, H. Patzelt, R. Ahlrichs, S. Spencer, A. Willets, *Phys. Chem. Chem. Phys.* **2006**, *8*, 1057–1065.
[47] W. L. F. Armarego, *Purification of Laboratory Chemicals*, Elsevier, Oxford, **2017**.
[48] P. S. Hallman, B. R. McGarvey, G. Wilkinson, *J. Chem. Soc. A* **1968**, 3143–3150.
[49] P. Hohenberg, W. Kohn, *Phys. Rev.* **1964**, *136*, B864–B871.
[50] Gaussian 16, Revision C.01, M. J. Frisch, G. W. Trucks, H. B. Schlegel, G. E. Scuseria, M. A. Robb, J. R. Cheeseman, G. Scalmani, V. Barone, G. A. Petersson, H. Nakatsuji, X. Li, M. Caricato, A. V. Marenich, J. Bloino, B. G. Janesko, R. Gomperts, B. Mennucci, H. P. Hratchian, J. V. Ortiz, A. F. Izmaylov, J. L. Sonnenberg, D. Williams-Young, F. Ding, F. Lipparini, F. Egidi, J. Goings, B. Peng, A. Petrone, T. Henderson, D. Ranasinghe, V. G. Zakrzewski, J. Gao, N. Rega, G. Zheng, W. Liang, M. Hada, M. Ehara, K. Toyota, R. Fukuda, J. Hasegawa, M. Ishida, T. Nakajima, Y. Honda, O. Kitao, H. Nakai, T. Vreven, K. Throssell, J. A. Montgomery, Jr., J. E. Peralta, F. Ogliaro, M. J. Bearpark, J. J. Heyd, E. N. Brothers, K. N. Kudin, V. N. Staroverov, T. A. Keith, R. Kobayashi, J. Normand, K. Raghavachari, A. P. Rendell, J. C. Burant, S. S. Iyengar, J. Tomasi, M. Cossi, J. M. Millam, M. Klene, C. Adamo, R. Cammi, J. W. Ochterski, R. L. Martin, K. Morokuma, O. Farkas, J. B. Foresman, and D. J. Fox, Gaussian, Inc., Wallingford CT, **2016**.
[51] O. V. Dolomanov, L. J. Bourhis, R. J. Gildea, J. A. K. Howard, H. Puschmann, *J. Appl. Crystallogr.* **2009**, *42*, 339–341.
[52] L. J. Bourhis, O. V. Dolomanov, R. J. Gildea, J. A. K. Howard, H. Puschmann, *Acta Crystallogr. Sect. A* **2015**, *71*, 59–75.
[53] G. M. Sheldrick, *Acta Crystallogr. Sect. A* **2008**, *64*, 112–122.
[54] G. M. Sheldrick, *Acta Crystallogr. Sect. A* **2015**, *71*, 3–8.

Manuscript received: May 25, 2023
Revised manuscript received: August 2, 2023
Version of record online: August 16, 2023